Chapter 5

Joining of C/SiC composites

A novel brazing formulation with carbon nanotube (CNTs) incorporated in the Ni-30Si alloy is designed to enhance the bonding of C/SiC composites. The LSS value and Rockwell hardness of the joint strongly depend on the amount of CNTs added. The joint with a 10 vol% CNTs content performs the best, with an average LSS value of 21 MPa, which is 147% higher than the joint prepared without the addition of CNTs. The enhancement in the joint strength is ascribed to the excellent wettability of filler, formation of new high-temperature resistant phases (e.g. Ni_2Si, Ni_3Si_2, and β-SiC) and a significant reduction in the CTE values causing lower thermal residual stresses while cooling. On the other hand, under excessive CNTs loading (>10 vol%), the joint strength is significantly diminished as a result of agglomeration, void formation, and poor wettability. The fracture surface analysis exhibited substantial CNTs rod pull-out, a phenomenon highly desirable for enhanced bond strength and non-catastrophic failure of the joint.

5.1 Introduction

Ceramic matrix composites (CMCs) attracted a great deal of attention due to their unmatched performance under severe operating conditions (Schmidt et al. 2004). CMCs, particularly carbon fibre-reinforced silicon carbide (C/SiC), have gained significance owing to their extraordinary thermal, mechanical, and thermo-mechanical properties (Bae et al. 2013). Therefore, C/SiC composites are lately preferred candidate materials in various applications such as aerospace (Buffenoir et al. 2016), nuclear (Salvo et al. 1996), automotive (Heinrich et al. 2001), and optical (Harnisch et al. 1998). Due to the inherent brittleness of ceramic materials, it is difficult to manufacture SiC components with large dimensions and intricate

shapes, which limits the range of applications for SiC ceramics (Dai et al. 2016). Several conventional and advanced techniques are available for joining CMCs with other metals and compounds (Li et al. 2009, Wan et al. 2019). Among these, brazing is a simple, efficient, and affordable joining technique.

The selection of an appropriate filler is crucial for maintaining the mechanical properties of the base material (Chen et al. 2015, Yang et al. 2018). Conventionally, commercially available Ag-Cu-Ti and Au-based fillers are employed in ceramics brazing due to their excellent wettability to SiC ceramic (Iwamoto et al. 1998, Dezellus et al. 2010). The reactivity of Ti could change the surface chemistry of the SiC ceramic by forming Ti_3SiC_2+Ti_5Si_3 layers and increasing the wettability of the molten filler on the SiC surface (Tillmanna et al. 2015). However, a considerable amount of brittle intermetallic compounds including Ti_3SiC_2, $TiSi_2$, and TiC are formed at the brazed joints due to the significant negative mixing enthalpies between the filler elements and Ti metals which seriously degrade the quality of the joints. Additionally, Ag-Cu-Ti fillers are expensive and susceptible to oxidation. As a result, their uses are constrained by weak joining strength at high temperatures and poor corrosion resistance (Patel et al. 2018). Sometimes, reactive metals (e.g. Ti, Mo, and Zr) are added to the fillers to facilitate the solid-state layer bonding of SiC-based composites (Morozumi et al. 1985, Singh et al. 2012). Notably, adding low CTE materials (particles or fibres) to the brazing filler metals may considerably decrease the thermal residual stress (TRS) of the joints (He et al. 2010). Consequently, the formation of high-temperature stable phases in the joint is desirable for high performance at high temperatures. Nonmetal fillers, including MAX ceramic, have recently received much attention due to their high-temperature performance, wear resistance, thermal shock resistance, and good plastic strain capacity. Ti_3SiC_2 is considered to be a potential choice among the several MAX phase ceramics for the joining of C/SiC composites (Zhang et al. 2009). Dong et al. reported the bonding of C/SiC composites utilising Ti_3SiC_2 filler at 1200–1600ºC and a pressure of 40 MPa (Dong et al. 2011). The maximum flexural strength of 110.4 MPa was obtained for the joint prepared at 1600ºC. Tatarko et al. investigated the CVD-SiC coating and without coating joining of C/SiC composites with a pre-sintered Ti_3SiC_2 foil employing the spark plasma sintering (SPS) technique at 1300ºC and a pressure of 50 MPa (Tatarko et al. 2016). The C/SiC composites coated with SiC exhibited maximum shear strength of 31.1 MPa, in comparison without the SiC coating (19.1 MPa). Although MAX ceramics offer excellent properties at high temperatures, their commercial applications have been constrained by the complexity of the synthesis process and the unavailability of highly pure commercial powders (Gonzalez-Julian

et al. 2021). Therefore, it is crucial to develop a novel filler for reliable pressure-less joining of the C/SiC CMCs for high-temperature applications.

Ni-based alloys have gained considerable interest due to their high thermal stability and excellent corrosion resistance. Numerous Ni-based corrosion-resistant alloys such as Ni-Mo (Hastelloy B), Ni-Cr-Mo (Hastelloy C), Ni-Cr-Fe (Inconel 600), and Ni-Cu (Monel 400) have been developed to date (Long et al. 2018). However, there haven't been many reports of brazing SiC ceramics with Ni-based anti-corrosion alloys. Shi et al. brazed GH3044 with SiC nanowire-toughened SiC coated C/C composites using Ni71CrSi brazing filler and reported the formation of Cr_7C_3+Ni_3Si phases, resulting in significant affinity between composite and Ni-based superalloys (Shi et al. 2017). To join sintered SiC ceramics, Wang et al. demonstrated that the Ni-Mo filler alloy exhibits remarkable wettability on SiC ceramics (Wang et al. 2021). The highest flexural strength of 174 MPa was realised at room temperature as a result of the formation of highly stable phases including Ni_3Mo_3C and Ni_2Si during brazing at 1300ºC for 40 min. Liu et al. investigated the wetting and adhesion behaviour of Ni-Si alloy on different substrates at high temperatures (Liu et al. 2010). They found that Si converts into thermally stable nickel silicide phases (e.g. Ni_2Si, Ni_3Si_2) and exhibits excellent wettability with the substrate. However, it has been observed that the production of brittle silicides and mismatch of CTE between Ni-Si-based intermetallics (>9 $\times 10^{-6}$/ºC) and C/SiC composites (3 $\times 10^{-6}$/ºC) often cause thermo-mechanical stresses. As a result, the joint is fundamentally weaker than the base materials, and fracture develops at the interface (Wen et al. 2018).

Carbon nanotubes (CNTs) have received a lot of interest recently due to their exceptional mechanical, electrical, and thermal properties. In particular, the CTE value of CNTs (1.9×10^{-6}/ºC) is closer to C/SiC composites ($3–5\times10^{-6}$/ºC); therefore, it can be a potential candidate in a reactive brazing filler formulation (Maniwa et al. 2001). Also, the crystalline ordered rod-like structure of CNTs, concerning the amorphous carbon fibre, ensures excellent stability at high temperatures. It has been shown that incorporating CNTs as a reactive filler in brazing materials enhances the joint strength and toughness, provides additional reinforcement due to the nanotube structure and resists the propagation of cracks by reducing the residual stresses at the interface (Zhou et al. 2017, Guo et al. 2019). During the joining of C/C composites, C reacts only with the braze material or the counterpart substrate; however, the brazing process is deemed even more complex in the case of C/SiC, as it involves diffusion and reaction of both C and SiC species (Yang et al. 2013, Tatarko et al. 2016].

The careful literature survey revealed that no report on the joining of C/SiC composites utilising CNTs-incorporated Ni-Si-based reactive braze material has been reported

yet. The majority of the work on joining C/SiC composites mentioned above was carried out either via SPS or diffusion bonding methods. However, these techniques are non-scalable to large-size components due to high temperature (>1500ºC), high pressure (>30 MPa), and complex brazing formulations. Therefore, the development of a simple, low-cost joining filler for bonding C/SiC composites to itself, which can render strong bonds under pressure-less brazing conditions is crucial. To this end, a low-cost reactive brazing formulation with CNTs incorporated in the Ni-30Si alloy is designed and employed for the joining of C/SiC composites at pressure-less conditions. CNTs content in Ni-30Si varied from 0 to 15 vol% in the brazing formulation. It has been found that the addition of CNTs to Ni-30Si alloy enhances the wettability with C/SiC while also lowering the CTE of the interlayer, which is advantageous for reducing the residual stress in the joints. The effect of CNTs content in Ni-Si braze on the strength of C/SiC-C/SiC bonds is investigated by evaluating lap shear strength (LSS). The microstructure of the joint interface and fracture surface is also studied through various characterisation techniques.

5.2 Experimental

An isothermal CVI-fabricated 2.5D C/SiC composite with a carbon fibre content of ~37 vol% and a density of 2.0 g/cc was utilised for joining studies. The carbon fabric preform was initially coated with pyrolytic carbon (PyC) interphase (~1 μm thick) followed by SiC infiltration using an 8 vol% methyltrichlorosilane-hydrogen mixture. The C/ SiC composite has an open porosity of 8–10 vol%, flexural strength of 350–370 MPa and inter-laminar shear strength of 22–24 MPa. Specimens were machined from C/SiC laminate using a diamond-coated cutting wheel.

Nickel (purity > 98%, $\bar{d}_p$=2.1 μm), silicon (purity > 98%, $\bar{d}_p$=5.3 μm) and multiwall carbon nanotubes (MWCNTs) (OD:30–80 nm and length: 10–50 μm) were procured from the commercially available sources. The filler composition was formulated by mixing the appropriate quantity of Ni, Si, and MWCNTs. It has been reported that Ni-Si alloys exhibit a non-reactive wetting behaviour over SiC surfaces if the percentage of Si is higher than 37 at.% (Rado et al. 1999). The Ni-Si phase diagram also reveals that at higher temperatures, Ni-rich phases (Ni_2Si, Ni_3Si_2, and Ni_5Si_2) are more stable than Si-rich phases (e.g. NiSi, $NiSi_2$) formed by high Si content (>30%) (Nash et al. 1987). Therefore, for this work, a Ni-Si alloy with a maximum of 30% silicon content was chosen as the brazing material to minimise the formation of low-temperature phases. The amount of MWCNTs varied from 0 to 15 vol%, and the

formulations prepared were designated as CNT-0, CNT-5, CNT-10, and CNT-15. The number in the nomenclature indicates the volume percentage of CNTs added to the formulation. The respective MWCNTs content, by weight, is also calculated and presented in Table 5.1. MWCNTs will henceforth be referred to as CNTs for the sake of brevity. The filler composition was prepared as well by substituting 10% of the CNTs in the Ni-Si alloy with graphite, and the resulting joint was designated as a Ni-Si-G joint to evaluate the effect of the morphology of the CNTs. The required amount of constituents was uniformly mixed using isopropyl alcohol in an agate jar, and the blending was performed in a planetary ball mill for up to 4 h, and subsequently dried at 80ºC under an inert atmosphere. A graphical illustration of the preparation of brazing alloy formulation and the joint is depicted in Fig. 5.1. The filler compositions along with thermal and wettability results are also presented in Table 5.1.

Table 5.1: Details of the brazing filler formulations

Filler Name	**CNTs (vol.%)**	**Avg. particle size (μm)**	**CTE (× 10^{-6} ºC)**	**Contact angle on C/SiC**
CNT-0	0 (0)*	2.8	13.6±0.5	130º
CNT-5	5 (1.6)	2.7	11.9±0.3	11º
CNT-10	10 (3.3)	2.2	8.3±0.3	17º
CNT-15	15 (5.2)	1.9	7.4±0.4	64º
Ni-Si-G	10 (3.3)	2.9	8.9±0.3	11º

**The bracketed quantity in the second column represents the corresponding weight basis.*

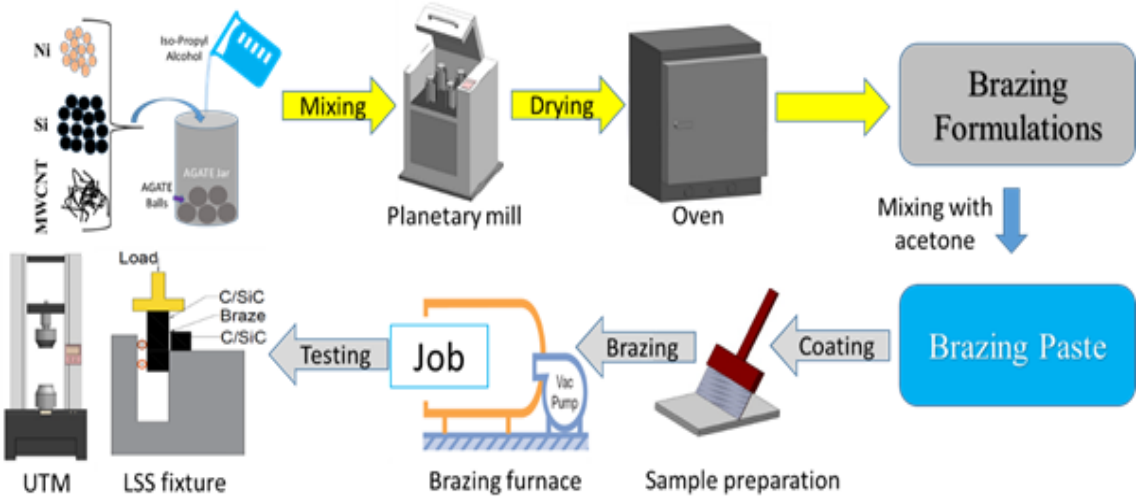

Fig. 5.1: Schematic for the processing of braze joints.

The bonding surfaces of C/SiC composites were polished with 320 SiC grit paper before being cleaned with an ultrasonic cleaner for 15 min in ethanol and dried in an oven at 150ºC. All four formulations (CNT- 0 to CNT-15) were mixed with acetone to make a paste. The paste was then applied using a brush in several layers to the connecting surfaces of the C/SiC composite to achieve the required coating thickness of ~200 μm. The coating was allowed to dry for 30 min at ambient conditions. The C/SiC composites were eventually placed into a vacuum brazing furnace that was maintained at 1350ºC with a 5ºC/min heating/cooling rate. To ensure good contact between joining surfaces, the brazing experiment was carried out at a dwell time of 30 min, a vacuum level of 10^{-5} mbar, and a dead load of 1 kg/cm^2. The bonded C/SiC specimens were designated J-CNT-0, J-CNT-5, J-CNT-10, and J-CNT-15, respectively.

The density of the brazing alloy powder was estimated using a specific gravity bottle as per ASTM D70–09. The average particle size ($\bar{d}_p$) of samples was measured using a subsieve auto sizer following ASTM B330. The DSC study was performed in an Ar environment at a 10ºC/min heating rate. The Ni-Si phase diagram, generated using Thermo-calc® software, was utilised to predict the theoretical melting point of each brazing formulation. To measure CTE, the brazing formulations were first heated at 1350ºC for 30 min and then pelletised to the dimension of 5mm×5mm×10mm in a cold press. The CTE was measured according to ASTM E-831, using a thermo-mechanical analyser (Make: TA Instruments, Model: TMA Q400) from 25 to 800ºC in an inert atmosphere.

A wettability study was conducted for all brazing formulations over C/SiC composite substrate at 1350ºC and a vacuum level of 10^{-5} mbar. The contact angle of droplets formed over the C/SiC composite substrate during the wetting experiment was characterised by an optical microscope (Make: Olympus).

The joint interfaces were tested for hardness using a Rockwell Tester, and the HRM scale (100 kgf load and a 1/4" ball) was used to calculate the Rockwell hardness. A coupon of two sizes-30 mm × 10 mm× 5 mm and 10 mm × 10 mm× 5 mm was cut to evaluate LSS and interfacial microstructural characterisations, respectively. The schematic for the LSS evaluation set-up along with testing equipment (Make: Instron, Model: UTM) is shown in Fig. 5.1. During the LSS test, the crosshead speed was maintained at 0.5 mm/min until the specimen was fractured. For each bonding experiment, three samples were analysed, and the average value was reported. The samples were mounted in transparent epoxy upto 140°C. Hot press epoxy mounted samples were polished to 1 μm grit finish using Carbimet cloth, Texmet C cloth, micro-cloth, micro-polishing suspension, and alumina suspension for the investigation

of the microstructure of the joint interface. The cross-section of bonded C/SiC composite was inspected by a scanning electron microscope (SEM) instrument (Make: Zeiss, Model: Supra 55) with an accelerating voltage of 15 kV. Energy dispersive spectroscopy (EDS) was used to analyse the elemental composition of specimens (Make: Bruker, Model: X Flash 6160). Phase characterisation was performed using an XRD (Make: Philips) by directing an X-ray beam at the sample through Cu-Kα radiation (λ = 1.5418 Å). The spectra were recorded at 25ºC with a step size of 0.02º and a time per step of 0.5 s.

5.3 Results and Discussion

5.3.1 Brazing Formulations Analysis

DSC tests were conducted up to 1400ºC in an argon environment to determine the melting characteristics of the Ni-Si-CNTs system, as illustrated in Fig. 5.2. The DSC analysis reveals that reactions happen in two distinct temperature zones, 870–1020ºC and 1250–1310ºC with a considerable energy change in the respective temperature regime. The exothermic peaks in the temperature regime of 870–1020ºC observed in all four cases can be attributed to the relaxation of amorphous structure and concurrent grain growth (Prasad et al. 2011). The endothermic peaks in the temperature range of 1250–1310ºC confirm the melting of filler (Nash et al. 1987). The addition of CNTs into Ni-30Si alloy caused a slight shift in melting range towards higher temperatures. The maximum change of 15ºC was observed in the case of CNT-15. As CNTs react with Si atoms, a certain amount of Si is consumed, and the alloy composition deviates from the eutectic point towards the lower Si side, causing an increase in the melting point (Nash et al. 1987, Li et al. 2020).

The theoretical melting point for each brazing composition is also estimated and marked in the Ni-Si phase diagram as shown in Fig. 5.3. This is the maximum limit which is predicted assuming the complete reaction of CNTs with Si. Therefore, it is anticipated that the experimental melting range for each brazing composition will be slightly away from the theoretically predicted value since Si can primarily react only with the surface carbon of CNTs (Taguchi et al. 2005). According to the phase diagram, the melting point can raise by 32ºC when CNTs up to 15% are used.

The brazing experiments were performed, for all types of fillers, at temperatures slightly higher than the upper limit of two regimes i.e. 1050ºC and 1350ºC to examine the feasibility of bonding. No joining was noticed due to the lack of melting, poor wettability, and

lack of filler reactivity with C/SiC composites at 1050ºC. Therefore, all brazing experiments were conducted at 1350ºC to ensure sufficient melting of the filler resulting in strong bonding.

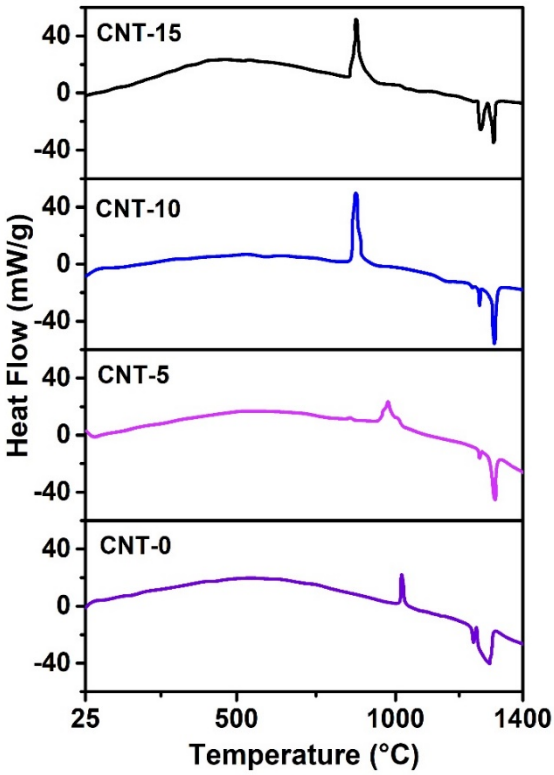

Fig. 5.2: DSC curves of brazing material formulations.

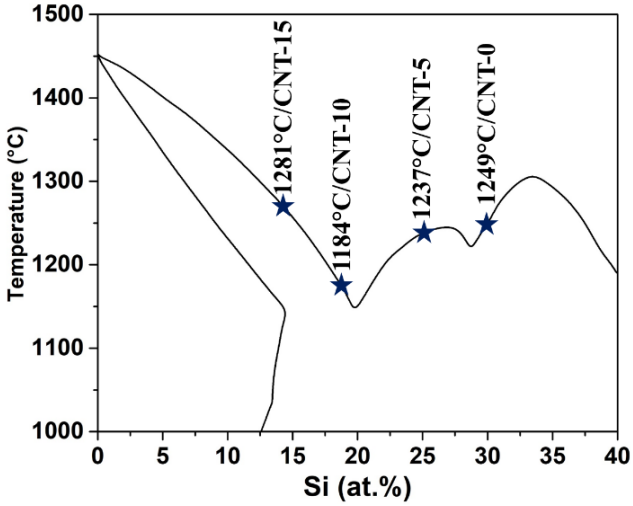

Fig. 5.3: Ni-Si phase diagram indicating the theoretical melting points for various brazing filler compositions.

Droplet images formed by the wettability experiment were taken into consideration for the contact angle measurements of brazing formulations on C/SiC composite substrate, as represented in Fig. 5.4.

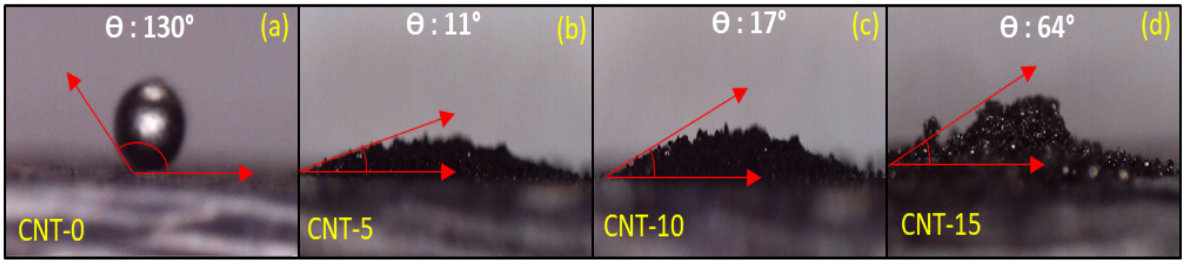

Fig. 5.4: Contact angle of (a) CNT-0, (b) CNT-5, (c) CNT-10, and (d) CNT-15 droplets on C/SiC substrate.

It can be observed that the contact angle of CNT-0 was as high as ~130º exhibiting very poor wettability over the C/SiC composites making it less suitable as the brazing material. After the addition of 5% CNTs, the contact angle of the alloy was drastically lowered to 11º. It has been observed that the presence of secondary wettable nanoparticles significantly alters the rheological characteristics of the composite solder alloys, causing a considerable reduction in the viscosity and surface energy of the melt (Xu et al. 2013, Zhang et al. 2014, Fathian et al. 2017). Moreover, the high reactivity of Si to CNTs also led to the formation of SiCNTs, a novel phase with excellent adhesive characteristics that offer less resistance to molten filler flowing over the CNTs surface. Li et al. also observed similar types of behaviour while investigating the effects of adding CNTs into Si-24Ti alloy for SiC monolith joints (Li et al. 2020). Therefore, it is expected that the viscosity and surface energy of molten Ni-Si alloy are significantly reduced as a result of the addition of CNTs. When CNTs content was increased to 10% (CNT-10), the contact angle of Ni-Si alloy slightly increased to 17º, demonstrating that increasing CNTs loading has a detrimental effect on wettability. However, as will be discussed in a subsequent section, the substantial formation of β-SiC and CNTs agglomeration resulted in a considerable rise in contact angle (64º) when the addition of CNTs increased above 10%. The increased concentration of β-SiC, as exhibited in the cases of CNT-10 and CNT-15, increases the contact angle and prevents the molten braze from flowing smoothly (Li et al. 2020). Therefore, the optimal addition of CNTs into Ni-30Si alloy is essential for obtaining good adhesive characteristics of the molten braze. As already stated, the significant thermal expansion mismatch between metal and composite has an immense adverse effect on the strength of the bonded joint and can even induce catastrophic failure. Consequently, CTEs of all formulations were measured from 25 to 800ºC, and the results are shown in Table 5.1. It appears that as the amount of CNTs in the braze increased, CTE values steadily reduced. This can be attributed to the low CTE of CNTs (1.9×10^{-6}/ºC) and the emergence of β-SiC as a new phase with a CTE value (~3×10^{-6}/ºC) that is comparable to that of the C/SiC composite.

5.3.2 Microstructure of the joint interface

The SEM images (not shown for brevity) of raw materials (Ni, Si, and CNTs) used for the brazing formulations reveal that Si particles have an uneven faceted structure, whereas Ni powders are aggregated, have a spherical shape, and CNTs bundles that were ruptured during the ball milling process have adhered to the surface of the Ni particle. Fig. 5.5 displays the SEM images and line scans of the C/SiC-C/SiC joints prepared by varying CNTs loading. All of the examples show an interface between the C/SiC substrates with a thickness of about 130–180 μm. As shown in Fig. 5.5a, the interface of J-CNT-0, the joint created without CNTs, is replete of cavities and fissures.

High- magnification SEM micrographs are also displayed in Fig. 5.6 to provide a better insight into the interface. The micrograph of J-CNT-0 (Fig. 5.6a) confirms the abundance of micro-cracks in the central zone of the interphase. Further magnification (inset of Fig. 5.6a) reveals that the smooth and continuous bulk phase of the central zone was separated by micro-cracks (as marked by arrows in Fig. 5.6a). It is interesting to note that while the bulk phase of the filler material is uniform and continuous with the presence of micro-cracks, the interface of filler-C/SiC tends to have large cavities and fissures. A line scan of the J-CNT-0 sample (Fig. 5.5b) shows only Ni and Si elements at the central zone, whereas all three elements are present on either side of the central zone.

An XRD analysis of the interface was carried out to identify the newly formed phases, as shown in Fig. 5.7. According to reactions (5.1) and (5.2), the central zone mainly consists of the Ni_2Si and Ni_3Si_2 phases, whereas the region on either side of it is recognised as an interface reaction zone (IRZ) wherein diffused Si and C from the C/SiC substrate primarily react with Ni and Si from the braze. At these brazing temperatures, no stable nickel carbides are formed; only the interactions between Ni-Si and Si-C are significant (Nam et al. 2021). It is anticipated that Ni and SiC react to form Ni_2Si and Ni_3Si_2 phases, releasing C atoms as per reactions (5.2) and (5.3) (Bhanumurthya et al. 2001). The free carbon then reacts with certain amounts of the Si in the braze, forming SiC following the reaction (5.4). The formation of SiC is expected only at IRZ, and its thickness is minimal (~25 μm) in the case of the J-CNT-0 sample. It is important to note that XRD confirms the formation of Ni_2Si and Ni_3Si_2 as primary phases. However, no peaks due to SiC were detected, possibly due to the negligible quantity of SiC formed in the case of the J-CNT-0 sample. Compared to the C/SiC composite, the nickel silicide phases have a higher CTE (13.6×10^{-6}/ºC for CNT-0) and lower ductility, mainly due to the Ni_2Si phase. As a result, after cooling, there are a lot of residual thermal stresses that

create voids and cracks at the interface, as seen in Fig. 5.5a and 5.6a (Mehan et al. 1979, Liu et al. 2010, Wen et al. 2018).

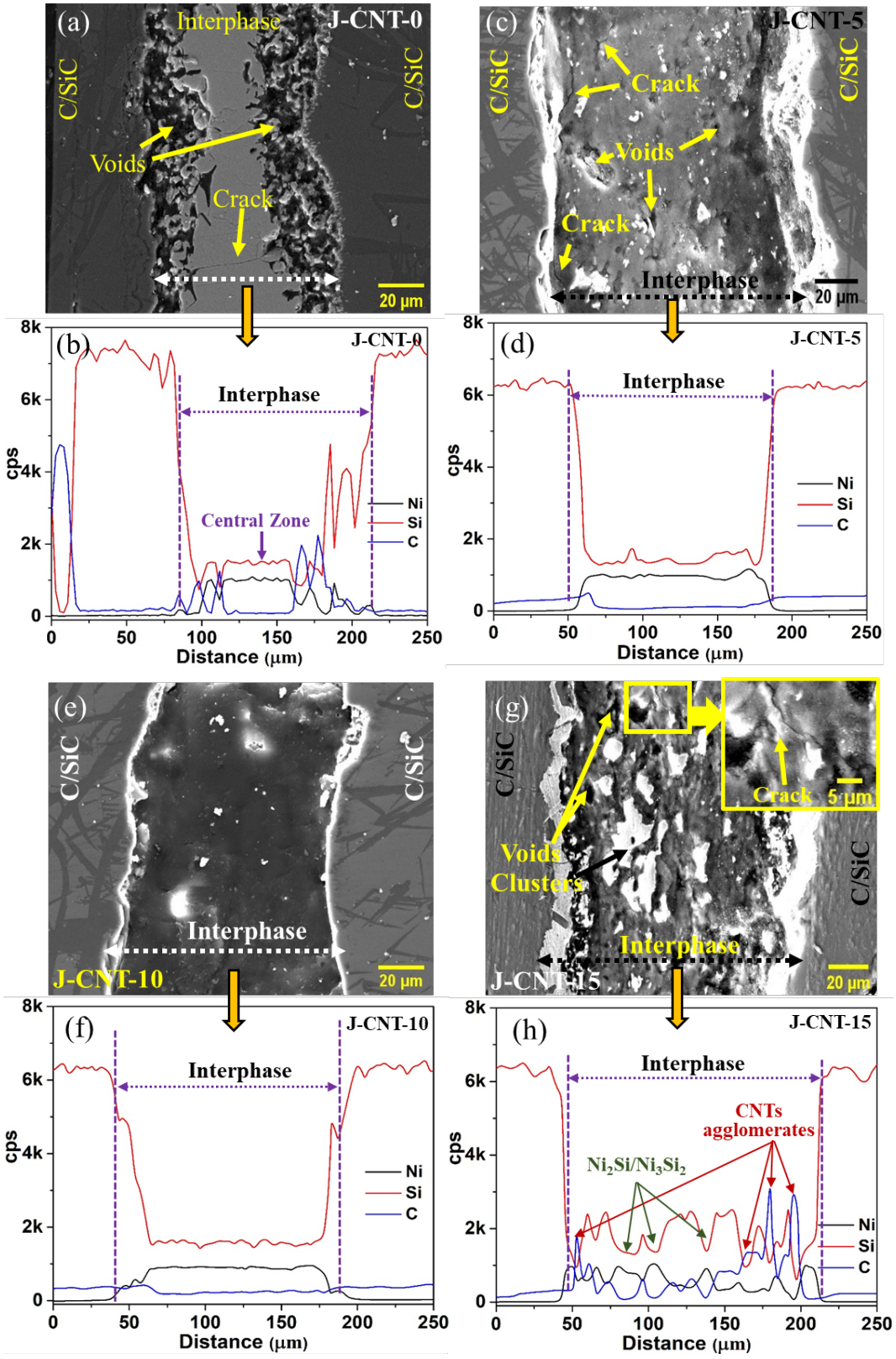

Fig. 5.5: SEM image and line scan of (a)-(b) J-CNT-0, (c)-(d) J-CNT-5, (e)-(f) J-CNT-10, and (g)-(h) J-CNT-15 joint interfaces.

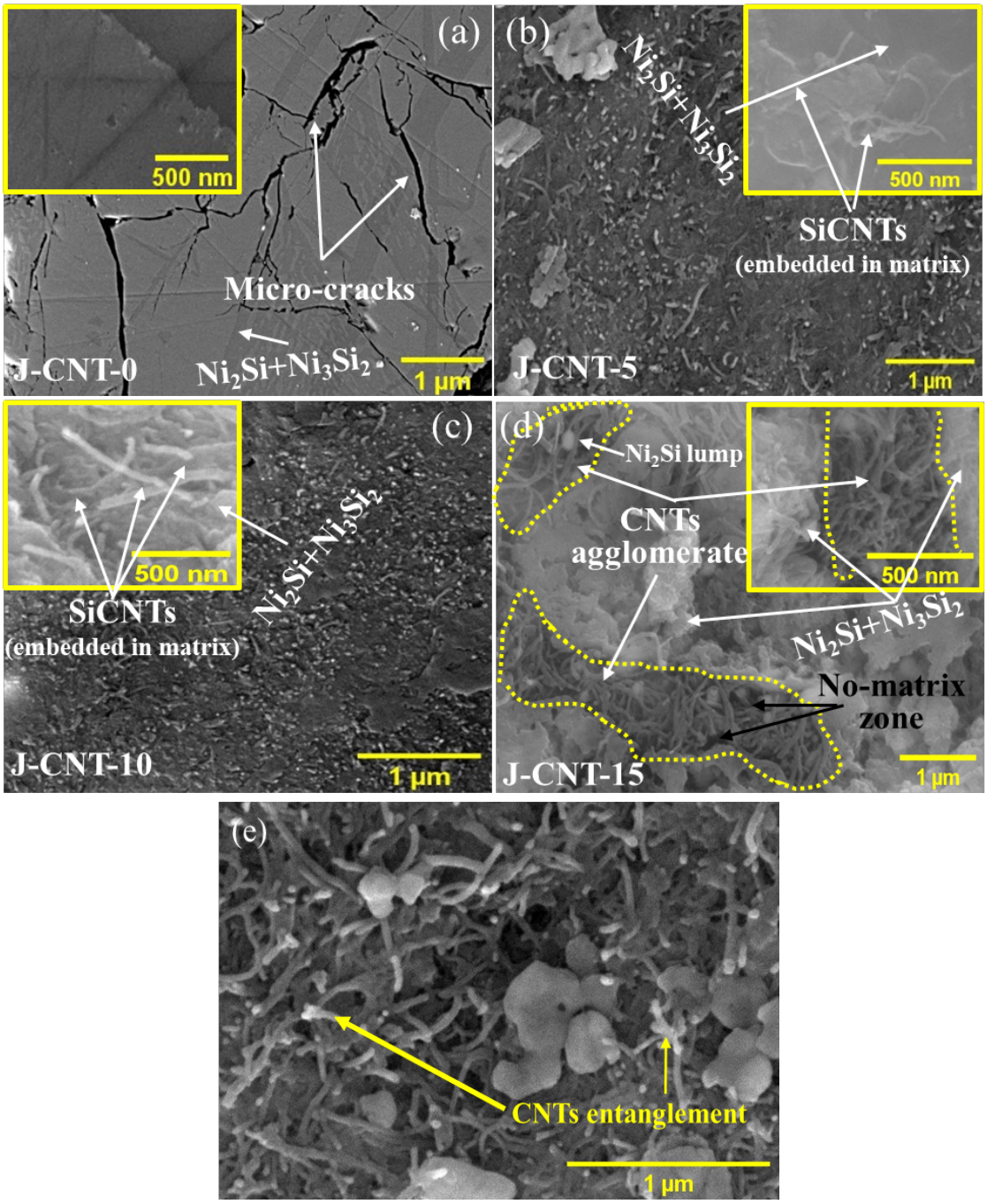

Fig. 5.6: High magnification SEM images of (a) J-CNT-0, (b) J-CNT-5, (c) J-CNT-10, (d)-(e) J-CNT-15 joint interfaces.

$$2Ni + Si \rightarrow Ni_2Si \qquad \Delta G = -45.05 \text{ kJ/mol} \qquad (5.1)$$

$$2Ni + SiC \rightarrow Ni_2Si + C \qquad \Delta G = -37.53 \text{ kJ/mol} \qquad (5.2)$$

$$3Ni + 2Si \rightarrow Ni_3Si_2 \qquad \Delta G = -44.84 \text{ kJ/mol} \qquad (5.3)$$

$$Si + C \rightarrow SiC \qquad \Delta G = -82.58 \text{ kJ/mol} \qquad (5.4)$$

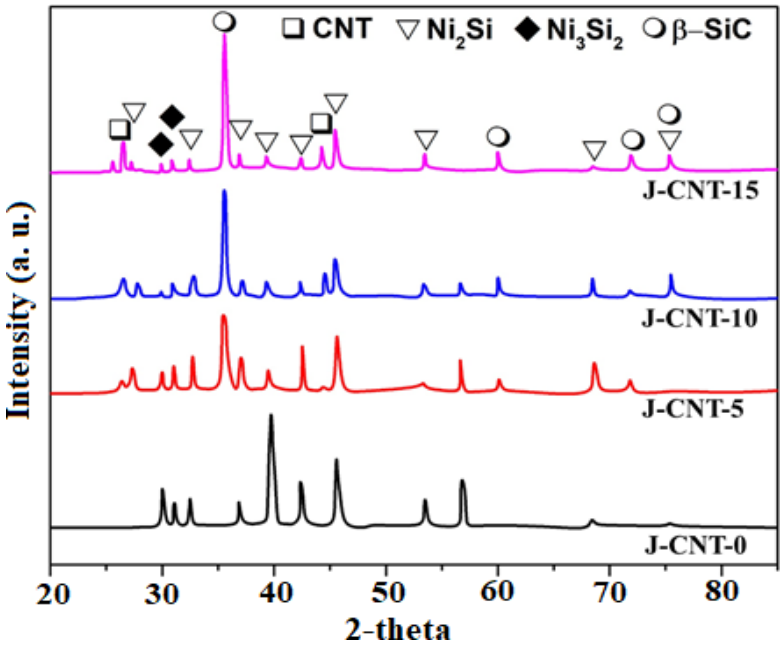

Fig. 5.7: XRD patterns of C/SiC-C/SiC joint interfaces.

The SEM micrograph of J-CNT-5 (Fig. 5.5c), compared to J-CNT-0, shows that the interface was more continuous, and the voids and cracks significantly decreased. The addition of CNTs into the Ni-30Si considerably modified the morphology and microstructure of the interface, as seen in Fig. 5.6b. The CNTs are well embedded in the braze filler and formed an integral part of the joint, confirming good wetting of CNTs by Ni-30Si alloy in line with the wettability results discussed earlier. Contrary to J-CNT-0, the interface of C/SiC composites adheres to both sides relatively well, and the region of defects is considerably reduced, demonstrating the beneficial effects of CNTs addition. High- magnification image (Fig. 5.6b) demonstrates that the CNTs are firmly embedded in the Ni-Si-derived matrix. The addition of CNTs lowered the overall CTE differences between the alloy and the substrate due to their incredibly low CTE, which remarkably decreased the number of voids, and cracks and reduced thermal stress. However, the joint (J-CNT-5) displayed a few macro-voids and cracks, as shown by the arrows in Fig. 5.5c, suggesting insufficient loading of CNTs to guarantee an imperfection-free joint.

Fig. 5.5e shows the SEM images of the cross-section of J-CNT-10. It is discovered that the C/SiC composites on either side are continuous and successfully integrated with the SiC substrate. In contrast to J-CNT-0 and J-CNT-5, the interface is utterly devoid of any imperfection, such as voids or cracks, demonstrating the superior quality of the C/SiC-C/SiC joint. Despite the increased number density of CNTs, their distribution is also relatively uniform for the J-CNT-10 (inset of Fig. 5.6c). Further, an increase in the CNTs concentration

to 15% developed a substantial amount of voids, cracks and deposits, as depicted in Fig. 5.5g for the J-CNT-15 joint. High-magnification SEM micrographs of J-CNT-15 (Fig. 5.6d) illustrate the irregular distributions of the Ni-Si-based compounds (white colour clusters) as confirmed by EDS. Agglomerates formed as a result of the CNTs aggregation were packed between the Ni-Si-based deposits (see Fig. 5.6d). This figure also confirms that the Ni-Si-based compounds have been embedded in the vicinity of aggregated CNTs, creating a sandwich-like structure at the interface. Additionally, a line scan of the interphase confirmed the formation of Ni-Si-based deposits and CNTs agglomerate at a few locations, as marked by arrows in Fig. 5.5h. EDS point analysis further demonstrates the production of the Ni_2Si+Ni_3Si_2 matrix and Ni_2Si lumps over the CNTs agglomerates at a few locations, as indicated by the marked arrows in Fig. 5.6d. The morphology of the J-CNT-15 interface may therefore be broadly classified into four groups: i) Ni_2Si+Ni_3Si_2 deposits, ii) CNTs agglomerates, iii) Ni_2Si lumps, and iv) 'no-matrix' zone. CNTs have an inherent problem of agglomeration and entanglement owing to their high aspect (L/D) ratio and the large Van der Waals forces (Cho et al. 2009). The agglomeration or entanglement phenomena are highly undesirable as they can act as the sites of stress concentration and crack generation, thereby hampering the envisaged beneficial effects. In addition, high loading of CNTs creates a shortage of the matrix material to wet the enormous surface area of the CNTs, which leads to lower flowability of filler metal and increases the propensity for the formation of voids, pores or agglomeration in the joint (Han et al. 2018). Consequently, high CNTs loading prevents the Ni-Si melt from wetting the entire CNTs surface area, leading to the development of a "no-matrix" zone and Ni_2Si lumps on top of it. Besides, a substantial amount of the molten Ni and Si was solidified locally over the agglomerates forming Ni_2Si+Ni_3Si_2-deposits around the CNTs agglomerates. The wetting experiments demonstrated that increasing the CNTs loading to 15% caused the contact angle to rise quickly to 64º and the interphase thickness to reach 180 μm.

The element distributions across cross-sections using EDS line scanning are displayed in Fig. 5.5. The scan indicates the presence of Ni, Si, and C in every joint except J-CNT-0. It is evident that Ni diffuses rapidly compared to Si towards the C/SiC substrate, Si reacts with remaining Ni and CNTs in the braze, and a 130–180 μm thick interlayer is formed between the substrates. Additionally, the IRZ could not be identified in joints prepared using CNTs (see line scans in Fig. 5.5d, f, and h), showing a uniform distribution of elements at the interface. However, in the case of J-CNT-0, since there was no carbon available within the filler, both Ni and Si diffused quickly in the direction of the C/SiC composites, leading to the development of IRZ. The hump on the extreme left side is caused by microscopic particles that may have

mistakenly stuck to the surface during the polishing or SEM sample preparation process. An XRD study of J-CNT-0 revealed that the unique phase Ni_2Si had been produced without the addition of CNTs. Contrarily, the CNTs-based joints suggested that novel phases of Ni_3Si_2 and β-SiC were also produced in addition to Ni_2Si according to the abovementioned reactions (Li et al. 2020).

5.3.3 Mechanical analysis

The LSS of C/SiC-C/SiC joints and the hardness of the respective brazed interlayer are presented in Fig. 5.8. The hardness value increased with the increase in CNTs loading and eventually approached the hardness of C/SiC composites (93.6 MPa). This could be attributed to the refined microstructure and the conversion of Si to β-SiC during the brazing process. The LSS value increased when CNTs were added to Ni- Si alloy up to 10%. It then decreases sharply with subsequent CNTs loading. A maximum LSS of 21 MPa was achieved for J-CNT-10, indicating good adhesion between the substrates. It is noticed that the LSS of J-CNT-0 is significantly lower than J-CNT-5 and J-CNT-10 due to excessive residual stresses generated by poor wetting and significant CTE mismatch between braze and C/SiC. It is interesting to note that the decrease in joint strength is dramatic and even less than J-CNT-0. It is well known that CNTs inherit strong intermolecular attraction behaviour due to high Van der Waals forces. As a result of this, when the CNTs content was increased to 15%, the entire surface area of the CNTs could not be adequately wetted by the molten braze, leading to tube-to-tube interactions. This eventually contributes to the formation of a complex network of CNTs through an entanglement (Fig. 5.6e), also known as clustering or bundling effect without any matrix (Reich et al. 2004, Rubel et al. 2019).

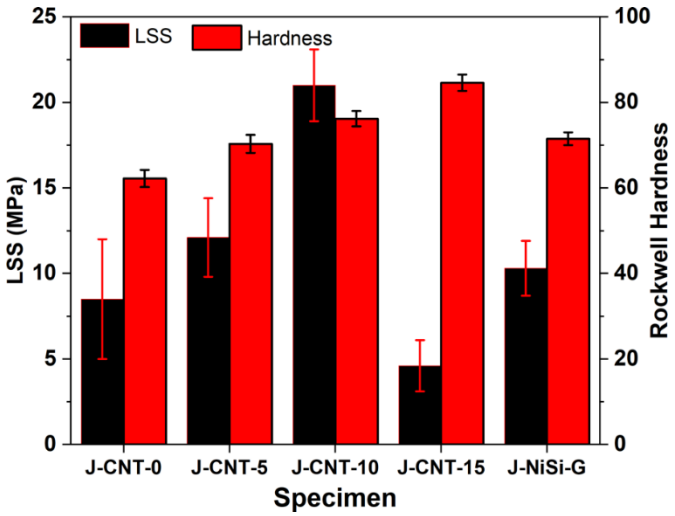

Fig. 5.8: LSS and Rockwell hardness of C/SiC-C/SiC joints.

The agglomeration is a more serious issue in the case of metal matrices including Ni or Si due to appreciable dissimilarities in density, electrostatic and Van der Waals forces in comparison to CNTs (Neubauer et al. 2010, Tian et al. 2018). Therefore, unlike J-CNT-0 where the interfaces were strongly connected despite voids, the matrix-less CNTs network in J-CNT-15 did not impart any strength to the joint. Additionally, this network emerged as the weakest region for stress concentration resulting in the production of cracks on the filler itself as opposed to at the C/SiC-filler interface for J-CNT-0 during the LSS test, as shown in Fig. 5.9d. As a consequence, the strength of J-CNT-15 significantly decreased, even below J-CNT-0. In conclusion, the addition of 10% CNTs into the Ni-30Si alloy (J-CNT-10) is optimum and renders the best joint strength due to the good wettability and interaction of the brazing material with the substrates.

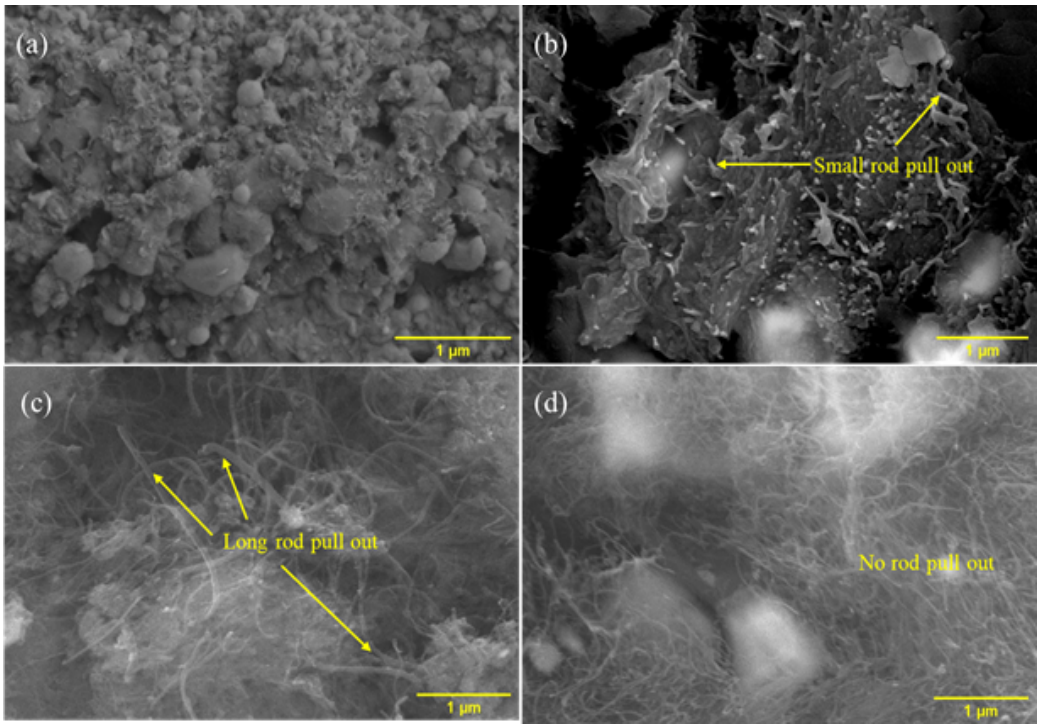

Fig. 5.9: SEM images of fracture surfaces of (a) J-CNT-0, (b) J-CNT-5, (c) J-CNT-10, and (d) J-CNT-15.

For the joining study, another kind of carbon, namely graphite, is also considered to understand the significance of the morphology of carbon sources in filler design. Since the best mechanical qualities were demonstrated by J-CNT-10, an equivalent amount of graphite was added to the Ni-30Si alloy to create the Ni-Si-G brazing formulation. The bonding of C/SiC composites (J-NiSi-G) was carried out using Ni-Si-G alloy by following the same procedure as those employed for CNTs-based ones. The wetting test of Ni-Si-G on the C/SiC composite revealed good wetting characteristics (contact angle:~11◦) similar to CNT-5 and CNT-10.

However, the LSS test of bonded C/SiC composites using Ni-Si-G demonstrated a maximum LSS of 10.3 MPa, much lower than the J-CNT-10 sample. Therefore, it can be argued that using CNTs as a carbon source in the filler is preferable to using other carbonaceous materials since it provide additional reinforcement to the joint because of its nanotube structure.

Following LSS analysis, Fig. 5.9 shows the fracture surface morphologies for various CNTs-reinforced Ni-30Si alloy-based joints. The random pattern on the braze and the lack of any visible C/SiC substrate suggest a brittle breakdown of the weakly bonded J-CNT-0 at the C/SiC- filler interface. The addition of CNTs substantially modified the morphology of the interface with the nano-rod-like structure. As indicated by the arrows in Fig. 5.9b and c, joints J-CNT-5 and J-CNT-10 show nano-rod pull-out. Interestingly, J-CNT-10 has a longer nano-rod pull-out length (~3 μm) than J-CNT-5 (~0.5 μm). When a bond is reinforced using CNTs, several mechanisms, including debonding, bridging, and pull-out, occur simultaneously during LSS testing, causing the joint to consume more energy and perform better under mechanical tests (Sarkar et al. 2016, Hajiaboutalebi et al. 2017). Consequently, moderate reinforcement content (~10%) improved interfacial bonding due to the lack of voids or agglomerates, which helped J-CNT-10 have the highest LSS value, as evidenced by the literature reported in Table 5.2. Due to the enormous surface area of CNTs, excessive CNTs loading inhibits the bonding of C/SiC by causing agglomeration, void formation, and a lack of matrix wetting. Therefore, the advantages of CNTs addition could not be realised, and consequently, J-CNT-15 exhibited a drastic reduction of up to ~78% in the LSS value.

Table 5.2: Literature reported shear strength of C/SiC-C/SiC joints by brazing process

Filler	Parameters	LSS (MPa)	Remarks	Ref.
Si	1410°C, 0-1 min	7	Low strength	Salvo 1996
Mo-Si	1450°C, 5-30 min, Ar	0	Low strength	Gianchandani 2016
Mo-Si-Mo	1450°C, 5-30 min, Ar	7-10	Low strength	Gianchandani 2016
Ni-Si-CNTs	1350°C, 30min, Vacuum	21	High strength	This work

5.3.4 Joining mechanism

The joining mechanism, namely reactive and non-reactive wetting, depends on the Si content of the Ni-Si-based system. McDermid et al. used solution thermodynamic theory to analyse the behaviour of the reaction between SiC ceramic and Ni-based alloy with varying Si

contents (McDermid et al. 1991). They discovered that alloys with Si contents above 37 at.% result in non-reactive joining, whereas alloys with Si contents below 37 at.% produce strong reactions at the interface. Therefore, the joining mechanism in the present study is reactive in nature as the Si content in all the alloys is below < 30 at.%. The joining mechanism of SiC ceramics using Si-based alloys has already discussed by previous authors (Zhou et al. 2015, Gianchandani et al. 2017, Li et al. 2020). The current work, however, emphasises how the wettability, microstructure evolution, and bonding response of the joint are modified by the addition of CNTs (0–15%) to the Ni-30Si-alloy.

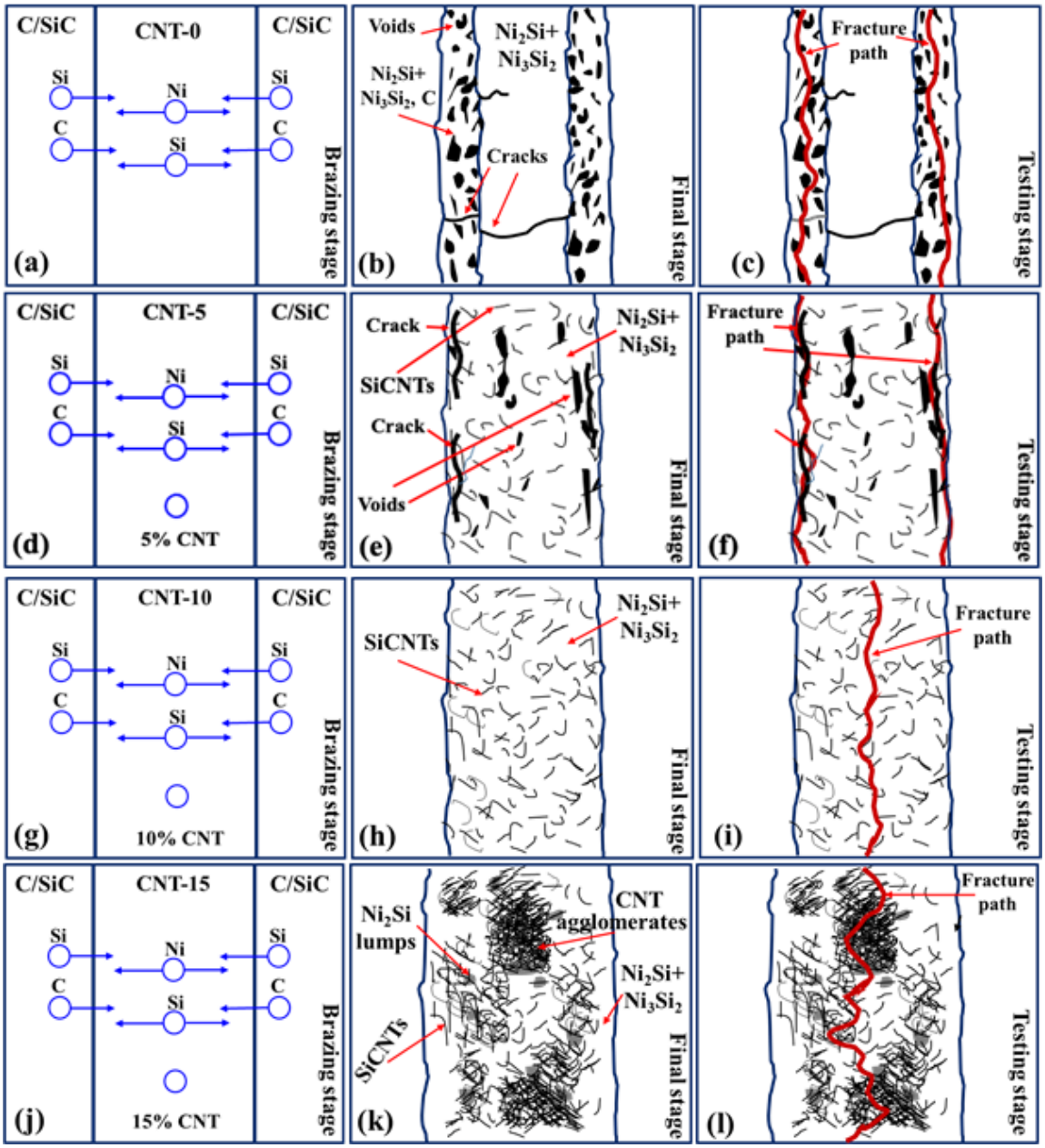

Fig. 5.10: Interface evolution model: (a)-(c) J-CNT-0, (d)-(f) J-CNT-5, (g)-(i) J-CNT-10, and (j)-(l) J-CNT-15.

Fig. 5.10 illustrates the evolution of joining interlayer microstructures and the fracture mechanism of the bonded specimens. The filler is initially sandwiched between the C/SiC composites, and then the brazing experiment is performed in a vacuum. The Ni-Si alloy melts, and Ni and Si diffuse into the C/SiC composites at brazing temperature (Fig. 5.10a-c). Ni preferentially reacts with SiC precipitating C atoms due to its low solubility in SiC and Ni-based silicides. Consequently, an IRZ of ~ 25 μm is formed at the interphase which is primarily composed of thermodynamically stable Ni_2Si+Ni_3Si_2 phases (Kaufman et al. 1979). Voids and cracks formed as a result of the large CTE mismatch between C/SiC and CNT-0 during the cooling process. The composites are nevertheless integrated with the aid of the flawed interlayer due to the strong bonding properties of SiC and Ni-Si-based compounds (Shi et al. 2020). During the LSS test, the fracture is produced primarily due to the presence of defects at the IRZ which are propagated further along the interlayer, leading to de-bonding between filler and substrate (Fig. 5.10c). The failure of the J-CNT-0 joint occurred in an adhesive mode.

The overall CTE is lowered to 11.9 × 10^{-6}/ºC by adding 5% CNTs to the filler, which reduces residual thermal stresses during cooling. The defects as a result significantly decreased, as illustrated in Fig. 5.10e. Ni_2Si+Ni_3Si_2 phases are created during the chemical reaction between Ni and SiC. It is also possible for Ni and Si to react with the CNTs in the filler. However, the reaction between Ni and CNTs to produce nickel carbides is thermodynamically not feasible due to a positive Gibbs free energy (40–50 kJ/mol) (Nam et al. 2021). Therefore, the reaction of Si atoms with the CNTs to produce β-SiC phases is favoured due to its lowest Gibbs free energy (− 82.58 kJ/mol). Over time, β-SiC wraps the core of CNTs, resulting in a co-axial Si-C nanotube (SiCNT) structure that has significantly better thermal and mechanical strength than CNTs (Taguchi et al. 2005, Malek et al. 2010). Although it is anticipated that this structure would reinforce the Ni_2Si+Ni_3Si_2 matrix at the interlayer, its content is not sufficient to eliminate the defects in the joint (Fig. 5.10e) and the undesirable adhesive-mode failure persists (Fig. 5.10f). The joint is discovered to be completely defect-free after increasing the CNTs loading to 10%, thanks to a 39% decrease in CTE value to 8.3 × 10^{-6}/ºC. The production of additional SiCNTs (Fig. 5.10h) and a substantially better-reinforced interlayer as a result of the higher CNTs number density led to a high LSS value, as shown by the extensive nano-rod pull-out (Fig. 5.9). This manifests in a change of failure mode to the desirable cohesive-mode (breakdown within the interlayer, Fig. 5.10i) with extensive SiCNTs pull-out. Even though increasing the CNTs loading to 15% further lowered the CTE value to 7.4 × 10^{-6}/ºC, the joint suffered from excessive CNTs agglomeration and Ni_2Si+Ni_3Si_2-based localised deposits (Fig. 5.10j and k) due to insufficient wetting of CNTs surface. As a result, during the LSS evaluation,

these locations served as the weakest points where the fracture started and spread (Fig. 5.10l), ultimately causing the joint to fail due to its extremely low mechanical strength (Dasilva et al. 2007). In summary, the J-CNT-10 joint, which is mainly composed of high-temperature phases like Ni_2Si, Ni_3Si_2, and SiCNTs, is microstructurally sound and has high mechanical strength.

5.4 Conclusions

In this study, novel carbon nanotubes (CNTs) reinforced Ni-Si-CNTs composite filler was developed to improve the mechanical properties and microstructure of a vacuum-brazed C/SiC-C/SiC joint. Ni-Si-CNTs alloy containing 10% CNTs exhibited good bonding for C/SiC composites and rendered the highest LSS (21 MPa) and Rockwell hardness (84.6) values, which is ~147% higher than the joint without CNTs addition. The microstructure analysis revealed that incorporating CNTs promotes the formation of new phases such as Ni_2Si, Ni_3Si_2, and β-SiC reducing the overall CTE mismatch and providing additional reinforcement to the interlayer. The joining of C/SiC without CNTs suffers from huge voids and cracks formation at the interface due to a significant difference in CTE between the C/SiC and the newly formed phases, specifically Ni_2Si. The loading above 10% significantly lowers the bond strength because of the poor wettability caused by the excessive agglomerates of CNTs, which creates voids and non-wettability issues in the joint. As a result, the LSS value of C/SiC-C/SiC joints prepared with an alloy containing 15% CNTs substantially decreases to 4.6 MPa. The proposed Ni-Si-CNTs system, with a good CTE match with the SiC matrix, is anticipated to show great potential as a joining material for pressureless joining SiC-based ceramic matrix composites.

References:

(1) B. Chen, H. Xiong, Y. Cheng, W. Mao, S. Wu, Microstructure and property of AlN joint brazed with Au-Pd-Co-Ni-V brazing filler, J. Mater. Sci. Technol. 31 (2015) 1034–1038, https://doi.org/10.1016/j.jmst.2014.11.026.

(2) B. Harnisch, B. Kunkel, M.Deyerler, S. Bauereisen, U. Papenburg, Ultra-lightweight C/SiC Mirrors and Structures, ESA Bull. 95 (1998).

(3) B. Nash, A. Nash, The Ni− Si (nickel-silicon) system, Bull. Alloy Phase Diagr. 8 (1987) 6–14, https://doi.org/10.1007/BF02868885.

(4) C. Iwamoto, S.I. Tanaka, Reactive wetting of Ag–Cu–Ti on SiC in HRTEM, Acta Mater. 46 (1998) 2381–2386, https://doi.org/10.1016/S1359-6454(98)80019-0.

(5) C. Rado, S. Kalogeropoulou, N. Eustathopoulos, Wetting and bonding of Ni-Si alloys on silicon carbide, Acta Mater. 47 (1999) 461–473, https://doi.org/ 10.1016/S1359-6454(98)00374-7.

(6) D. Han, H. Mei, S. Xiao, K.G. Dassios, L. Cheng, A review on the processing technologies of carbon nanotube/silicon carbide composites, J. Eur. Ceram. Soc. 38 (2018) 3695–3708, https://doi.org/10.1016/j.jeurceramsoc.2018.04.033.

(7) E. Neubauer, M. Kitzmantel, M. Hulman, P. Angerer, Potential and challenges of metal-matrix-composites reinforced with carbon nanofibers and carbon nanotubes, Compos. Sci. Technol. 70 (2010) 2228–2236, https://doi.org/10.1016/j. compscitech.2010.09.003.

(8) F. Buffenoir, C. Zeppa, T. Pichon, F. Girard, Development and flight qualification of the C–SiC thermal protection systems for the IXV, Acta Astronaut. 124 (2016) 85–89, https://doi.org/10.1016/j.actaastro.2016.02.010.

(9) G.W. Liu, F. Valenza, M.L. Muolo, A. Passerone, SiC/SiC and SiC/Kovar joining by Ni-Si and Mo interlayers, J. Mater. Sci. 45 (2010) 4299–4307, https://doi.org/ 10.1007/s10853-010-4337-3.

(10) H. Dong, S. Li ,Y. Teng, W. Ma, Joining of SiC ceramic-based materials with ternary carbide Ti_3SiC_2, Mater. Sci. Eng. B 176 (2011) 60–64, https://doi.org/10.1016/j.mseb.2010.09.002.

(11) H. Long, S. Mao, Y. Liu, Z. Zhang, X. Han, Microstructural and compositional design of Ni-based single crystalline superalloys - a review, J. Alloy. Compd. 743 (2018) 203–220, https://doi.org/10.1016/j.jallcom.2018.01.224.

(12) H. Shi, Y. Chai, N. Li, J. Yan, X. Zhu, K. Chen, D. Bai, Z. Liu, M. Wu, R. Zhang, M. Li, M. Luo, Q. Sun, C. Xin, W. Hu, X. Dong, Interfacial reaction mechanism of SiC joints

joined by pure nickel foil, J. Eur. Ceram. Soc. 40 (2020) 5162–5171, https://doi.org/10.1016/j.jeurceramsoc.2020.07.048.

(13) H.B. Zhang, Y.W. Bao, Y.C. Zhou, Current status in layered ternary carbide Ti_3SiC_2, a review, J. Mater. Sci. Technol. 25 (2009) 1–38. https://www.jmst.org/EN/abstract/abstract8407.shtml.

(14) J. Cho, A.R. Boccaccini, M.S.P. Shaffer, Ceramic matrix composites containing carbon nanotubes, J. Mater. Sci. 44 (8) (2009) 1934–1951, https://doi.org/ 10.1007/s10853-009-3262-9.

(15) J. Gonzalez-Julian, Processing of MAX phases: from synthesis to applications, J. Am. Ceram. Soc. 104 (2021) 659–690, https://doi.org/10.1111/jace.17544.

(16) J. Li, L. Liu, Y. Wu, Z. Li, W. Zhang, W. Hu, Microstructure of high-temperature Ti based brazing alloys and wettability on SiC ceramic, Mater. Des. 30 (2009) 275–279, https://doi.org/10.1016/j.matdes.2008.04.070.

(17) J. Yang, J. Huang, Z. Ye, S.H. Chen, R. Ji, Y. Zhao, Influence of interfacial reaction on reactive wettability of molten Ag-Cu-X wt% Ti filler metal on SiC ceramic substrate and mechanism analysis, Appl. Surf. Sci. 436 (2018) 768–778, https://doi.org/10.1016/j.apsusc.2017.12.106.

(18) J.C. Bae, K.Y. Cho, D.H. Yoon, S.S. Baek, J.K. Park, J.I. Kim, D.W. Im, D.H. Riu, Highly efficient densification of carbon fiber-reinforced SiC-matrix composites by melting infiltration and pyrolysis using polycarbosilane, Ceram. Int. 39 (2013) 5623–5629, https://doi.org/10.1016/j.ceramint.2012.12.078.

(19) J.G. Heinrich, F. Aldinger, Ceramic materials and components for engines, in R. Gadow, M. Speicher (Eds.), Multilayer C/SiC Composites for Automotive Brake Systems, Wiley-VCH, 2001, pp. 565–570, https://doi.org/10.1002/ 9783527612765.ch96.

(20) J.R. McDermid, R.A.L. Drew, Thermodynamic brazing alloy design for joining silicon carbide, J. Am. Ceram. Soc. 74 (1991) 1855–1860, https://doi.org/ 10.1111/j.1151-2916.1991.tb07799.x.

(21) K. Bhanumurthya, R. Schmid-Fetzer, Interface reactions between silicon carbide and metals (Ni, Cr, Pd, Zr), Compos. A Appl. Sci. Manuf. 32 (2001) 569–574, https://doi.org/10.1016/S1359-835X(00)00049-X.

(22) K. Malek, M. Sahimi, Molecular dynamics simulations of adsorption and diffusion of gases in silicon-carbide nanotubes, J. Chem. Phys. 132 (2010), 014310, https://doi.org/10.1063/1.3284542.

(23) K. Sarkar, S. Sarkar, P.K. Das, Spark plasma sintered multiwalled carbon nanotube/silicon carbide composites: densification, microstructure, and tribo- mechanical characterization, J. Mater. Sci. 51 (2016) 6697–6710, https://doi.org/ 10.1007/s10853-016-9956-x.

(24) L. Kaufman, Coupled phase diagrams and thermochemical data for transition metal binary systems-VI, CALPHAD 3 (1979) 45–76, https://doi.org/10.1016/0364-5916 (79)90020-8.

(25) L. Tian, L. Zheng, L. Ren, Q. Chen, Future prospects of carbon nanotubes reinforced metal matrix composite, Res. Dev. Mater. Sci. 3 (2018) 226–228, https://doi.org/ 10.31031/RDMS.2018.03.000555.

(26) L. Zhang, K.N. Tu, Structure and properties of lead-free solders bearing micro and nanoparticles, Mater. Sci. Eng. R Rep. 82 (2014) 1–32, https://doi.org/10.1016/j. mser.2014.06.001.

(27) L.F.M. Dasilva, T.N.S.S. Rodrigues, M.A.V. Figueiredo, M.F.S.F. Demoura, J.A. G. Chousal, Effect of adhesive type and thickness on the lap shear strength, J. Adhes. 82 (2007) 1091–1115, https://doi.org/10.1080/00218460600948511.

(28) M. Hajiaboutalebi, M. Rajabi, O. Khanali, Physical and mechanical properties of SiC-CNTs nano-composites produced by a rapid microwave process, J. Mater. Sci. Mater. Electron. 28 (2017) 8986–8992, https://doi.org/10.1007/s10854-017- 6629-8.

(29) M. Patel, V. Singh, S. Singh, V.V. Bhanu Prasad, Micro-structural evolution during diffusion bonding of C-SiC/C-SiC composite using Ti interlayer, Mater. Charact. 135 (2018) 71–75, https://doi.org/10.1016/j.matchar.2017.11.031.

(30) M. Salvo, M. Ferraris, P. Lemoine, M.A. Montorsi, M. Merola, Joining of CMCs for thermonuclear fusion applications, J. Nucl. Mater. 233 (1996) 949–953, https:// doi.org/10.1016/S0022-3115(96)00148-1.

(31) M. Singh, T. Matsunaga, H.T. Lin, R. Asthana, T. Ishikaw, Microstructure and mechanical properties of joints in sintered SiC fiber-bonded ceramics brazed with Ag–Cu–Ti alloy, Mater. Sci. Eng. A 557 (2012) 69–76, https://doi.org/10.1016/j. msea.2012.05.110.

(32) M. Xu, H. Liu, H. Zhao, W. Li, How to decrease the viscosity of suspension with the second fluid and nanoparticles? Sci. Rep. 3 (2013) 3137, https://doi.org/10.1038/ srep03137.

(33) M. Yang, L. Zhang, X. Tian, Y. Liu, P. He, J. Feng, Interfacial microstructure and mechanical properties of TiAl and C/SiC joint brazed with TiH_2–Ni–B brazing powder, Mater. Charact. 79 (2013) 52–59, https://doi.org/10.1016/j. matchar.2013.02.010.

(34) M.J.N.V. Prasad, A.H. Chokshi, On the exothermic peak during annealing of electrodeposited nanocrystalline nickel, Scr. Mater. 64 (2011) 544–547, https://doi.org/10.1016/j.scriptamat.2010.11.038.

(35) O. Dezellus, R. Voytovych, A.P.H. Li, G. Constantin, F. Bosselet, J.C. Viala, Wettability of Ti_3SiC_2 by Ag–Cu and Ag–Cu–Ti melts, J. Mater. Sci. 45 (2010) 2080–2084, https://doi.org/10.1007/s10853-009-3941-6.

(36) P. Tatarko, V. Casalegno, C. Hu, M. Salvo, M. Ferraris, M.J. Reece, Joining of CVD- SiC coated and uncoated fibre reinforced ceramic matrix composites with pre- sintered Ti_3SiC_2 MAX phase using Spark Plasma Sintering, J. Eur. Ceram. Soc. 36 (2016) 3957–3967, https://doi.org/10.1016/j.jeurceramsoc.2016.06.025.

(37) P. Wan, M. Li, K. Xu, H.B. Wu, K.K. Chang, X.B. Zhou, X.D. Ding, Z.R. Huang, H. X. Zong, Q. Huang, Seamless joining of silicon carbide ceramics through an sacrificial interlayer of $Dy_3Si_2C_2$, J. Eur. Ceram. Soc. 39 (2019) 5457–5462, https://doi.org/10.1016/j.jeurceramsoc.2019.09.002.

(38) P.K. Gianchandani, V. Casalegno, F. Smeacetto, M. Ferraris, Pressure-less joining of C/SiC and SiC/SiC by a MoSi2/Si composite, Int. J. Appl. Ceram. Technol. 14 (2017) 305–312, https://doi.org/10.1111/ijac.12631.

(39) R.I. Rubel, M.H. Ali, M.A. Jafor, M.M. Alam, Carbon nanotubes agglomeration in reinforced composites: a review, AIMS Mater. Sci. 6 (2019) 756–780, https://doi.org/10.3934/matersci.2019.5.756.

(40) R.L. Mehan, R.B. Bolon, Interaction between silicon carbide and a nickel-based superalloy at elevated temperatures, J. Mater. Sci. 14 (1979) 2471–2481, https://doi.org/10.1007/BF00737038.

(41) S. Morozumi, M. Endu, M. Kikuchi, K. Hamajima, Bonding mechanism between silicon carbide and reactive metals, J. Mater. Sci. 20 (1985) 3976–3982, https://doi.org/10.1007/BF00552387.

(42) S. Nam, H.W. Lee, I.H. Jung, Y.M. Kim, Microstructural characterization of TiC-reinforced metal matrix composites fabricated by laser cladding using FeCrCoNiAlTiC high entropy alloy powder, Appl. Sci. 11 (2021) 6580, https://doi.org/10.3390/app11146580.

(43) S. Reich, C. Thomsen, J. Maultzsch, Carbon nanotubes-basic concepts and physical properties, Chem Phys Chem 5 (2004) 1914–1915, https://doi.org/10.1002/cphc.200400387.

(44) S. Schmidt, S. Beyer, H. Knabe, H. Immich, R. Meistring, A. Gessler, Advanced ceramic matrix composite materials for current and future propulsion technology applications, Acta Astronaut. 55 (2004) 409–420, https://doi.org/10.1016/j. actaastro.2004.05.052.

(45) T. Taguchi, N. Igawa, H. Yamamoto,Synthesis of silicon carbide nanotubes, J. Am. Ceram. Soc. 88 (2005) 459–461, https://doi.org/10.1111/j.1551- 2916.2005.00066.x.

(46) W. Guo, H. Zhang, W. Yuan, Y. Zhu, H. Zhang, P. Peng, B. Qi, F. Li, The microstructure and mechanical properties of C/C composite/Ti_3Al alloy brazed joint with graphene nanoplatelet strengthened Ag-Cu-Ti filler, Ceram. Int. 45 (2019) 8783–8789, https://doi.org/10.1016/j.ceramint.2019.01.203.

(47) W. Tillmanna, J. Pfeiffera, N. Sieversa, K. Boettcher, Analyses of the spreading kinetics of AgCuTi melts on silicon carbide below 900ºC, using a large-chamber SEM, Colloids Surf. A 468 (2015) 167–173, https://doi.org/10.1016/j. colsurfa.2014.12.039.

(48) X. Dai, J. Cao, Z. Chen, X. Song, J. Feng, Brazing SiC ceramic using novel B_4C reinforced Ag–Cu–Ti composite filler, Ceram. Int. 42 (2016) 6319–6328, https:// doi.org/10.1016/j.ceramint.2016.01.021.

(49) X. Shi, X. Jin, H. Lin, J. Jing, L. Li, C. Wang, Joining of SiC nanowires-toughened SiC coated C/C composites and nickel based superalloy (GH3044) using $Ni_{71}CrSi$ interlayer, J. Alloy. Compd. 693 (2017) 837–842, https://doi.org/10.1016/j. jallcom.2016.09.245.

(50) X.B. Zhou, Y.H. Han, X.F. Shen, et al., Fast joining SiC ceramics with Ti3SiC2 tape film by electric field-assisted sintering Technol, J. Nucl. Mater. 466 (2015) 322–327. https://doi.org/10.1016/j.jnucmat.2015.08.004.

(51) Y. Maniwa, R. Fujiwara, H. Kira, H. Tou, E. Nishibori, M. Takata, M. Sakata, A. Fujiwara, X. Zhao, S. Iijima, Y. Ando, Multiwalled carbon nanotubes grown in hydrogen atmosphere: an x-ray diffraction study, Phys. Rev. B 64 (2001), 073105, https://doi.org/10.1103/PhysRevB.64.073105.

(52) Y. Zhou, D. Liu, X. Song, J. Liu, Y. Song, Z. Wang, J. Feng, Characterization of carbon/carbon composite/Ti6Al4V joints brazed with graphene nanosheets strengthened AgCuTi filler, Ceram. Int. 43 (2017) 16600–16610, https://doi.org/ 10.1016/j.ceramint.2017.09.049.

(53) Y.M. He, J. Zhang, Y. Sun, C.F. Liu, Microstructure and mechanical properties of the Si3N4/42CrMo steel joints brazed with Ag–Cu–Ti+Mo composite filler, J. Eur. Ceram. Soc. 30 (2010) 3245–3251, https://doi.org/10.1016/j.jeurceramsoc.2010.07.005.

(54) Z. Fathian, A. Maleki, B. Niroumand, Synthesis and characterization of ceramic nanoparticles reinforced lead-free solder, Ceram. Int. 43 (2017) 5302–5310, https://doi.org/10.1016/j.ceramint.2017.01.067.

(55) Z. Li, R. Wei, Q. Wen, Z. Zhong, K. Song, Y. Wu, Microstructure and mechanical properties of SiC ceramic joints vacuum brazed with in-situ formed SiC particulate reinforced Si-24Ti alloy, Vacuum 173 (2020), 109160, https://doi.org/10.1016/j.vacuum.2019.109160.

(56) Z. Wen, Y. Zhao, H. Hou, L. Chen, First-principles investigation of mechanical and thermodynamic properties of nickel silicides at finite temperature, Phys. Solid State 60 (2018) 967–974, https://doi.org/10.1134/S1063783418050360.

(57) Z.Wang,Y.Liu,H.Zhang,J.Jiang,T.Lin,X.Liu,Z.Huang,JoiningofSiCceramics using the Ni-Mo filler alloy for heat exchanger applications, J. Eur. Ceram. Soc. 41 (2021) 7533–7542, https://doi.org/10.1016/j.jeurceramsoc.2021.07.056.